Finite element modelling on the effect of the height-to-diameter ratio of bilayer iron powder compact

Syamimi Mohd Yusoff (cikmimi88@gmail.com)
Universiti Putra Malaysia
Suraya Mohd Tahir
Universiti Putra Malaysia
Azmah Hanim Mohammed Ariff
Universiti Putra Malaysia
Eris Elliandy Supeni
Universiti Putra Malaysia
Mohd Shamsul Anuar
Universiti Putra Malaysia

Research Article

Keywords: Finite element, density gradient, bilayer compact, height-to-diameter ratio, local RD distributions, iron powder

Posted Date: April 13th, 2022

DOI: https://doi.org/10.21203/rs.3.rs-1542469/v1

Abstract

In this study, finite element modelling (FEM) had been implemented to capture the changes in interfacial local relative density (RD) distribution between compressed layers of a green bilayer iron powder compact system. Validation work had been taken as an initial work before undergoing several modelling tests on different green bilayer iron compacts with specified height-to-diameter (H/D) ratios. Our proposed experimental framework with a new mapping technique was used to gather the details of RD distribution on a real green single (Sample A1) and a bilayer iron sample (Sample A2). We produced the desired experimental local RD distribution under a magnification of 100X via an optical microscope and visualization through Tecplot software. An effective prediction on local RD distribution on single green iron powder compacts allowed for further assumption in layered samples. To proceed, four kinds of H/D ratios of 1.0 (Sample A2), 1.3 (Sample B), 1.6 (Sample C) and 1.9 (Sample D) were assigned for layers with the same thickness. Via modelling, observation on the highest interfacial local RD distribution had been successfully captured for H/D ratios of 1.0, followed by 1.3 and 1.6. It had been revealed that the green bilayer iron powder compacts efficiently delivered its densification as well as minimization on its density gradient compared to the green single iron powder compact.

Introduction

Powder compaction is a central processing stage of Powder Metallurgy (PM). It draws substantial attention from metallurgists owing to the fact that the strength of the green iron powder compact produced affects the integrity of the final PM product. An abundance of past literature had reported findings, either through experimental [1, 2] or modelling [3] strategies, to work out the effect of compaction parameters on the mechanical properties of green iron powder as well as add-ons of the material model [2] to ensure flexible predictions. Investigations have been focused on the sintering stage since it is part of the PM process before going into the secondary and machining processes as the final operation [4, 5]. Specifically, reducing the non-uniformity of density gradients and flaws that cause the deterioration of samples is necessary from the early stage of PM processes. One of the methods to overcome these natural flaws is through the layering strategy. The addition of successive layers of compaction can uplift the quality of the compressed powder sample. Hence, the layered-based method for PM production has become a blueprint for all kinds of powders since it has a high potential of being implemented in diverse areas. Experimentally, a bilayer structure of compressed powder is attainable by a sequential compression of two (or dual) types of powder [6] and one (or mono) type of powder [7]. Recently, for example, in the orthopaedic application, Ti6Al4V-based bilayer samples have been practised for bone implants [8]. Significantly, its major applications are beneficial to enhance the properties of machining tools [6].

To date, mono-based bilayer powder compact has not been widely studied in the research of PM. In the case of green iron powder, prominent research was performed by Sopchak and Misiolek [9] using double-sided compaction. Experimentally, they had carried out green and sintered iron powder compaction up to eight layers with 107 MPa compaction pressure from the top and bottom punches. The results of their

qualitative-based assessment were presented via distributed greyscale images. Through hardness measurement, they evidently captured elevation in hardness in the middle of the compressed region. From their findings, they recommended that the production of more than one layer of iron-based powder compact holds large potential in compensating the robustness of PM-based production by further reducing the density gradients with an increasing height of the layer. Based on their experiment, delamination had been highlighted around the upper region, causing the separation of the uppermost layer from a compressed body. Concerning this detrimental issue, it is necessary to assess the response of interfacial properties against the double variation of uniaxial compaction load. With the advancement of computational tools, it becomes possible to meticulously retrieve local relative density (RD) distribution quantitatively. Since local RD distribution is denoted as a solution-dependent variable (SDV), consequent variables that represent the mechanical properties of green iron powder compact can be analysed in detail.

In summary, there are two ways of modelling bilayer powder compaction, namely the two-step compaction modelling [7, 10] and simultaneous compaction modelling [11]. The former modelling procedure involves imposing uniaxial compaction two times, resembling the experimental procedure to form a bilayer, whereas the latter involves imposing uniaxial compaction load on two undeformed layers of green powder compact at the same time. Most dual-based bilayer powder compacts can be modelled under simultaneous action. For mono-based compact, the modelling procedure can be done using the two-step compaction.

In this current work, simultaneous compaction modelling was used. Nevertheless, it is noteworthy to mention that in the finite element analysis (FEA), the tracking of effects on local RD distribution across the joining interface between two similar types of powder by successively increasing compaction load under a one-sided method has never before been documented. Hence, suitable input parameters must be chosen so that numerical convergence in the mesh analysis can be achieved since this bilayer powder analysis has not been encountered in any past literature. Besides, the Brewin equations [12] were intercalated for the first time in a common material model, namely the Cap Plasticity.

Material And Methods

Development of the finite element model

We had systematically implemented the Modules of Abaqus under Explicit mode including Part, Assembly, Property, Step, Interaction, Load and Mesh Modules which were performed consequently as listed in Table 1. Lastly, submission of Job was done to run the powder compaction model with the employment of an explicit subroutine. Under Part and Assembly Modules, as shown in Fig. 1, each layer was made of deformable shell CAX4R element whereas the die and pair of punches were fixed as meshed wire, together with a rigid RAX2 element under an asymmetrical model. Following the experimental dimensions, each layer of powder was initialized as 1 cm, the length of upper and lower punches was 0.5 cm each whereas the die wall was set as 2 cm.

For Property Module, the behaviour of densification for each iron powder layer was assessed through the implementation of built-in Cap Plasticity whereby the data input was produced with the integration of material properties proposed by Brewin et al. [12]. The input data is listed in Table 2. RD is the ratio of current RD to full RD. The initial and full local RD distribution for green iron compact was 0.5 and 1.0, respectively, and each of iterated RD values was 0.02. The size of mesh for each tri-based element was set as 0.1 for both Fig. 1(a) and (b) with the total number of seeding for Fig. 1(b) located at the interface being 110 for the Mesh Module. Therefore, the modelled green iron powder is more flexible to compress two layers without mesh distortion. A series of modelling steps had been assigned under the Step Module with an initial step and followed by a second step (named Step-1). Each step computed the history and output of strain, axial and von Mises stresses and SDV. Step-1 restored all History and Field Variable Outputs from the initial step to update each determined variable for visualization later in an output database (ODB) file.

In the Interaction Module, the global friction coefficient under a penalty value of 0.08 was set for interaction between the die wall and the green iron powder, indicating the modelled condition for the lubricated die compaction process [13]. On the other hand, a penalty value of 0.5 was set between the green iron powder and other rigid surfaces including upper and lower punches since no lubricant was applied on the top and bottom die parts. Next, we determined the boundary conditions (BCs) for each step in the Load Module. In order to enforce static condition on the applied lower punch and die wall, it is important to select ENCASTRE condition and assign it as Reference Point 1 (RP1) located at the points between the lower punch and an asymmetrical line as well as Reference Point 2 (RP2) located at a point on the die wall. In connection with the initial step, Reference Point 3 (RP3) of the upper punch was set as zero under the selection of displacement or rotation option. Consequently, during the operation of Step-1, RP3 was then displaced downward under a vertical direction based on the set value.

Table 1: A series of Abaqus Modules used in the current work.

Abaqus Modules						
	Part and Assembly	Property	Mesh	Step	Interaction	Load
	Die	Cap Plasticity	Tri-based elements	Initial Step — BC-1, BC-2, BC-3	Die wall- Powder	Boundary Conditions
	Upper Punch				Powder-Powder	
	Lower Punch	Brewin Equations		Step 1 — BC-1, BC-2, BC-3, BC-4	Upper Punch-Powder	
	Upper Layer of Iron Powder				Lower Punch-Powder	
	Lower Layer of Iron Powder					

Table 2
Lists of input parameters of Cap Plasticity to model the green bilayer iron powder compact

Young Modulus K (MPa)	Poisson Ratio v	Cohesion d (MPa)	Angle of friction $tan\,\beta$	Cap eccentricity R	Yield stress p_b (MPa)	Plastic Strain ϵ^{pl}	Local RD
5644.120	0.0556	0.001	72.48784	0.56465685	12.89	0	0.5
7752.250	0.0607	0.2485472	72.05262	0.57774487	24.78	0.3738570	0.55
16317.06	0.0909	3.0391120	70.85212	0.66822970	110.1	0.6150191	0.7
21301.68	0.1059	6.1909922	70.47973	0.72582784	165.8	0.6840119	0.75
29109.18	0.1234	12.040375	70.11856	0.80407416	242.6	0.7485505	0.8
42633.40	0.1433	22.486328	69.76742	0.90835824	346.2	0.8091751	0.85
68727.35	0.1658	40.517986	69.42531	1.04501934	483.6	0.8663335	0.9
125703.4	0.1907	70.717656	69.09136	1.22144311	662.9	0.9204007	0.95
270046.3	0.2182	119.94670	68.76484	1.44616171	893.7	0.9716940	1

Sample preparation for the validation of the finite element model

Iron powder (Hoganas ASC 100.29) had been selected with magnesium stearate as its lubricant. The one-sided pressing step was performed using a universal testing machine (model 3382, Instron, UK) having a 100 kN maximum capacity load cell to produce a green single layer and a bilayer iron powder compact.

Figure 2 illustrates the step formation for the green single layer and bilayer iron powder compacts. The sample for the single layer (Sample A1) had been prepared starting from Fig. 2(a), the filling of loose iron powder with an initial height and mass of 1 cm and 10 grams respectively. Next, a compaction load of 95 kN was applied (Fig. 2(b)), followed by the ejection of the green single layer iron powder compact in Fig. 2(e).

In addition to the steps shown in Figs. 2(a), 2(b) and 2(e) for Sample A1, the steps shown in Figs. 2(c) and 2(d) were added in the preparation of the bilayer powder compact (Sample A2). Both the compaction for lower and upper layers in Figs. 2(b) and 2(d) were accomplished by compaction loads of 30 kN and 95 kN respectively. A crosshead speed of 5 mm/min was used to enhance the compressibility that had been specialized for the formed interface during the compaction stage. This, theoretically, delivers low potential in elastic energy for compressed layers from delamination. Next, to produce a sample with less delamination, an ejection speed of 2 mm/min was implemented to reduce the impact from the container on its bottom part, as shown in Fig. 2(e). This implementation was expected to balance the stress state

distribution during and after the ejection stage. Then, the obtained cylindrical-shaped samples with a thickness of 0.5 cm for Sample A1 and 1.0 cm for Sample A2 were cross-sectioned following the arranged procedures under a metallographic technique in Fig. 3. The captured surfaces were finally indicated in Figs. 4(a) and 4(b).

Quantitative image analysis for the green single layer and bilayer iron powder compacts

To obtain the final local RD distribution across the cross-section of the green single layer and bilayer iron compacts as in Figs. 4(a) and 4(b), a systematic preparation according to the workflow process of the quantitative image analysis from Stage (1) to Stage (4) shown in Fig. 3 was used for validation with the finite element model. Stage (1) can be represented as per Figs. 2(a), 2(b), 2(c), 2(d), and 2(e). The details of Stages (2) and (3) were according to the previous work of the author [14] with a low ejection speed.

Height variation for simulation on the effect of Height-to-Diameter (H/D) ratio

The H/D ratio is the geometrical indicator that refers to the effectiveness in the escalation of height (H) corresponding to the strength of interface under a constant value of diameter (D) for the layered system of the green metal powder compact. A robust bilayer structure would deliver local RD distribution at its interface nearer to full density or local RD distribution of 1.0 with elevated height [9]. In this work, three different H/D ratios were employed to study its effect on the density gradient across the powder compact and the pattern of local RD distribution around the interface. As seen in Table 3, samples A2, B and C were compacted with the same load of 30 kN and 95 kN on the lower and upper layers, respectively, to examine the effect of the H/D ratio.

Table 3
List of H/D ratio under compaction load on lower (30 kN) and upper (95 kN) layers.

Samples	H/D ratio	Compaction load on lower layer (kN)	Compaction load on upper layer (kN)
A2	1.0	30	95
B	1.3	30	95
C	1.6	30	95
D	1.9	30	95

Results And Discussion

As a result, differences in distributed local RD distribution within the internal cross-sections of the green single layer (Sample A1) and bilayer (Sample A2) iron powder compacts can be observed. Based on the physical appearance on the left side of Figs. 4(a) and 4(b), we noticed that the mirror-like area was

apparently visible across the whole and around the middle of the cross-sectioned green single layer and bilayer samples respectively. On the other hand, the dark-coloured area was interpreted as an area with scattered voids or known as porosities. This can be seen on the edge corner of the lowermost region of Sample A1. This may occur due to its less impact from load compaction. Whereas for Sample A2, all area surrounding the formed interface between the two layers, particularly the lowermost region of the cross-sectioned surface, was scattered by voids. This was caused by particles sliding and re-arranging due to the densification occurred that at the interface. Also, the lowermost region displayed randomly scattered voids that received equally less impact due to their positions being farther from the impact of the upper punch and the immobile lower punch.

From our detailed examination through quantitative image analysis, we finally retrieved the local RD distribution on the right-hand side of Figs. 4(a) and 4(b). The green single layer sample exhibited a relative density in the range between 0.93 and 0.99, whereas the green bilayer sample exhibited a relative density in the range between 0.9 and 0.99.

Validation of the finite element model

In FEM, the green single layer of Sample A1 and bilayer iron powder compact of Sample A2 were displayed in an axisymmetric form due to their compaction under the same geometrical perspective as represented in Fig. 5 and Fig. 6.

As indicated in Figs. 5(a) and 5(b), we had made a comparable local RD distribution between experimental (left) and modelling (right) works on the green iron powder compact. For Fig. 5(a), the highest position of the powder region was occupied by the highest local RD distribution followed by the middle and bottom regions under experimental results. Through FEM, the same contour had been obtained whereby the uppermost corner, middle and lowermost corner regions had closer values corresponding to experimental results with RD values of 0.99, 0.96 and 0.93 respectively. With the addition of a layer in Fig. 5(b), the experimental results had displayed changes in the contour of RD distribution, particularly at the interfacial region of the examined cross-section. The highest position of the powder region located at the uppermost corner was occupied by the highest local RD distribution followed by the middle and bottom regions. The middle region that had formed the interface between two compressed green iron powders experienced the most increase of RD values compared to the upper and lower parts as they are nearer to the upper and lower punches, respectively. The RD value between the uppermost corner and interfacial regions was calculated as 0.98. In comparison with FEM, the same contour level had been successfully obtained. As indicated in FEM results, the uppermost and lowermost corner regions were displayed as 0.99 and 0.9 of RD values to experimental results respectively. The simulated interfacial regions were indicated to agree with an RD value of 0.9765. Therefore, the distributed RD results of the experiment are finally validated with FEM as all regions were in agreement.

Effect of HD ratio on the density gradient and RD distribution

In this section, we discovered the difference in local RD distribution on the cross-sections of the green single (left of Fig. 6) and bilayer iron powder compacts (right of Fig. 6).

In Fig. 6(a), the green single and bilayer iron powder of Sample A1 and Sample A2 respectively displayed some differences in the RD contour. Upon the final compaction stage, the uppermost and lowermost corner of the green bilayer iron had shown the RD values of 0.9844 and 0.9131 Whereas for the green single layer iron, the uppermost and lowermost corner had also displayed closer to full RD of 1.0, that is, 0.9852 and 0.9126 respectively. The result of the RD contour for the green bilayer iron had significantly delivered an enhancement of RD distribution around 0.9777 at the interfacial region between the two compressed layers. It possessed the second-highest RD value after the uppermost corner region since it was under the connected flow due to the nesting response from the lower layer as well as from the effect of friction from the die wall.

As seen in Fig. 6(b) with Sample B under a H/D ratio of 1.3, the green bilayer iron exhibited the highest local RD distribution at the uppermost corner, followed by the uppermost corner of the green single layer iron with RD values of 0.9921 and 0.9541 respectively. However, the green single layer iron had the lowest distributed local RD located at the lowermost corner, then the second-lowest value was denoted at the lowermost corner of the green bilayer iron with RD values of 0.8757 and 0.9171 respectively. Notice that on the cross-section of the green bilayer iron, with the addition of the same initial mass and thickness as in its lower layer, we can observe the increment of local RD distribution around the interfacial area upon the final compaction stage. As such, an equal amount of area of both upper and lower parts of the interfacial region received the same distributed RD values in the range between 0.9851 and 0.9781. In contrast, the local RD values were averagely distributed along the cross-section of the green single layer iron with the highest local RD distribution realized within the smallest region at the uppermost corner that was affected by the die wall friction.

In Fig. 6(c) with Sample C under a H/D ratio of 1.6, the green bilayer iron exhibited the highest local RD distribution at the uppermost corner with an RD value of 0.9994 compared to the full local RD value of 1.0. The lowermost region of the green bilayer iron displayed an RD value of 0.9239. Whereas for the green single layer iron, the highest and lowest local RD values were reported to visualize at the uppermost and lowermost regions by 0.9769 and 0.8850 respectively. Per contra to the green bilayer of Sample B from Fig. 6(b), the distributed interfacial RD of the green bilayer iron of Sample C in Fig. 6(c) was seen to slightly disperse on the lower part of the interfacial region. Nevertheless, the interfacial region of the green bilayer iron is covered by higher local RD distribution compared to the green bilayer iron in Fig. 6(b). It is in the range between 0.9923 and 0.9852.

As observed on the right side of Fig. 6(d) for Sample D under a H/D ratio of 1.9, the green bilayer iron exhibited the highest local RD distribution at the uppermost corner compared to the full distributed local RD of 1.0 within the smallest region. It is worth noting that the distributed RD values were not effectively emerged across the interfacial region as the powder height is increased. It is in the range between 0.977 and 0.9692. For the lowermost region of green bilayer iron, it displayed an RD value of 0.9539 whereas

the green single layer iron showed the lowest distributed RD at the uppermost and lowermost regions of its cross-section with a difference of RD values of 0.9964 and 0.8791 respectively.

Therefore, it was revealed that the formation of higher densification can possibly be visualized via Abaqus/Explicit with the compaction values of 30 kN and 95 kN done on the lower and upper layers respectively with the same thickness. The cross-section of the green single layer iron had shown a standard decrement of local RD distribution from the uppermost corner to the lowermost corner region, with averagely distributed local RD along the mid-region under a fixed lubricant condition of 0.08. This is due to the fact that the pressure flow is gradually ineffective as it is transferred towards the bottom of the powder compact. Meanwhile, the effect from double compaction had covered the interfacial region of the green bilayer iron with higher distributed local RD under H/D ratios of 1.0, 1.3 and 1.6. However, beginning with the increased powder height to H/D ratio of 1.9, this effect no longer rises. As a result, the local RD distribution was decreased around the interface.

Overall, it was denoted that the distributed RD values at the uppermost corner of the green bilayer iron remained higher compared to the green single layer iron for all H/D ratios. This was attributed to the friction impact from the upper punch and die. Moreover, the assemblage of recent loose iron powder from the upper layer with the lower layer during a period of second compaction may uphold the increment of RD values around the uppermost corner of the compressed green bilayer iron. Similarly, the lowermost corner region of the green bilayer iron remained higher compared to the green single layer iron for all H/D ratios. This was attributed to the double impact from the upper punch for the formation of the green bilayer iron powder compact. The resulting density gradient and changes in the interfacial local RD distribution between the green single and bilayer irons will be analysed in the next section.

Based on Fig. 7(a), the density gradients of the green single and bilayer iron powder compacts were compared. We noticed that the increment of H/D ratio up to 1.9 had increased the density gradient under lubricated die conditions. This can be described by an increase of local RD values for all H/D ratios, particularly at the uppermost corner of the green single layer ranging from 0.9852 to 0.9964 whereas the lowermost corner values ranged from 0.9126 to 0.8791. Whereas, less gradient had been displayed by final values of RD for the green bilayer iron at the uppermost corner ranging from 0.9844 to 1. Similarly, for the lowermost corner, the RD values ranged from 0.9131 to 0.9165. From these findings, we can deduce that the implementation of lubricant is beneficial for the process of compaction, especially for the green bilayer powder compact in strengthening the interfacial region through the obtained RD values. Also, the global friction coefficient of 0.08 in FEA modelling was proved to be reliably implemented in the simulation of compaction, thus correctly determining the density evaluation based on previous validation.

By increasing the H/D ratio to observe the resulting interfacial local RD distribution, we obtained Fig. 7(b). The increase of the values occurred starting from a H/D ratio of 1.0 to 1.6. However, the reduction of the values had taken place for the highest H/D ratio of 1.9. Since the impact from the upper punch was further from the interface of the green bilayer iron with incremental values of H/D ratio, the dependence of the interfacial region to be densified by the upper punch was less and was barely enhanced by the

compactness between the two layers with increased mass as well as barely affected by the gravitational force. Nevertheless, it had been proved that the gradient of all green bilayer iron powder compacts was less compared to the compacted green single powder with the same height.

Conclusions

Based on our experiment and modelling observation, the compaction of double layers shows promising enhancement on local RD distribution around the interfacial regions as visualized in Abaqus/Explicit. As a consequence, it can be proven that by employing increased H/D ratios, the density gradient can be lowered by layering strategy under lubricated die conditions. Therefore, the H/D ratio and layer thickness are prioritizing factors that are responsible for the production of a strong layered system. With the validation from FEM, the need for a trial-and-error method can be reduced, and material costs can be saved. Overall, the application of Cap Plasticity with material properties proposed by Brewin et al. [12] can successfully capture the interfacial evolution. Thus, it can be further explored to recognize the details of mechanical-related parameters in facilitating the observation of other failure mechanisms or defects.

Declarations

Acknowledgements

The authors acknowledge the lab tutorial supports provided by the Strength of Material Laboratory, Faculty of Engineering, Universiti Putra Malaysia (UPM), Malaysia.

Funding information. This work was supported by IPS Putra Grant (GP-IPS/2019/9654100). The corresponding author has received research support from Universiti Putra Malaysia (UPM), Malaysia.

Conflicts of interest/Competing interests. The authors have no relevant financial or non-financial interests to disclose.

Availability of data and material.

Code availability. An association of commercial finite element Abaqus 6.20 software and custom research code is written in Fortran 90: on request, the author will make the code available.

Ethics approval. Not applicable

Consent to participate. Not applicable

Consent for publication. In The International Journal of Advanced Manufacturing Technology

Authors' contributions. Syamimi Mohd Yusoff is a PhD student. She was involved in experimental and modelling of bilayer iron powder compact, validation and writing the original draft. Dr. Suraya Mohd Tahir

and Dr. Shamsul Anuar assisted in review the whole article. Dr. Azmah Hanim is examined the metallographic technique. Dr. Eris Elliyandi is examined the modelling technique.

References

[1] Alabi AA, Tahir SM, Zahari NA et al (2017) A modified diametrical compression test technique (MDCTT) for mode II fracture toughness of iron powder compact, Powder Technol. 319:356-364.

[2] Zadeh HK (2010) Finite element analysis and experimental study of metal powder compaction. PhD Thesis, Queen's University.

[3] Tahir SM, Ariffin AK, Anuar MS (2010) Finite element modelling of crack propagation in metal powder compaction using Mohr–Coulomb and Elliptical Cap yield criteria, Powder Technol. 202:162-170.

[4] Favrot N, Besson J, Colin C, Delannay F (1999) Cold Compaction and Solid- State Sintering of WC- Co-Based Structures: Experiments and Modeling, J Am Ceram Soc. 82:1153-1161.

[5] Boonyongmaneerat Y, Schuh CA (2006) Contributions to the interfacial adhesion in cosintered bilayers, Metall Mater Trans A. 37:1435-1442.

[6] Ojo-kupoluyi OJ, Tahir SM, Ariff AHM et al (2017) Densification rate and interfacial adhesion of bilayer cemented tungsten carbide and steel, Int J Mater Res. 108:1090-1098.

[7] Yohannes B, Gonzalez M, Abebe A et al (2017) Discrete particle modeling and micromechanical characterization of bilayer tablet compaction, Int J Pharmaceut. 529:597-607.

[8] Téllez-Martínez JS, Olmos L, Solorio-Garcia VM et al (2021) Processing and characterization of bilayer materials by solid state sintering for orthopedic applications, Metals-Basel. 11:207.

[9] Sopchak ND, Misiolek WZ (2000) Density gradients in multilayer compacted iron powder parts, Mater Manuf Process. 15:65-79

[10] Sinka C (2007) Modelling powder compaction, Kona Powder Part J. 25:4-22.

[11] Rowe JM, Nikfar F (2017) Modeling approaches to multilayer tableting, In Predictive Modeling of Pharmaceutical Unit Operations, Woodhead Publishing.

[12] Brewin PR, Coube O, Doremus P, Tweed JH (2008) Modelling of powder die compaction. Springer, London.

[13] Zhou M, Huang S, Hu J et al (2017) A density-dependent modified Drucker-Prager Cap model for die compaction of Ag57. 6-Cu22. 4-Sn10-In10 mixed metal powders, Powder Technol. 305:183-196.

[14] Yusoff SM, Tahir SM, Azmah Hanim MA et al (2021) Fabrication and evaluation of density distribution in green bilayer iron powder compact, Mater Manuf Process. 36:660-667.

Figures

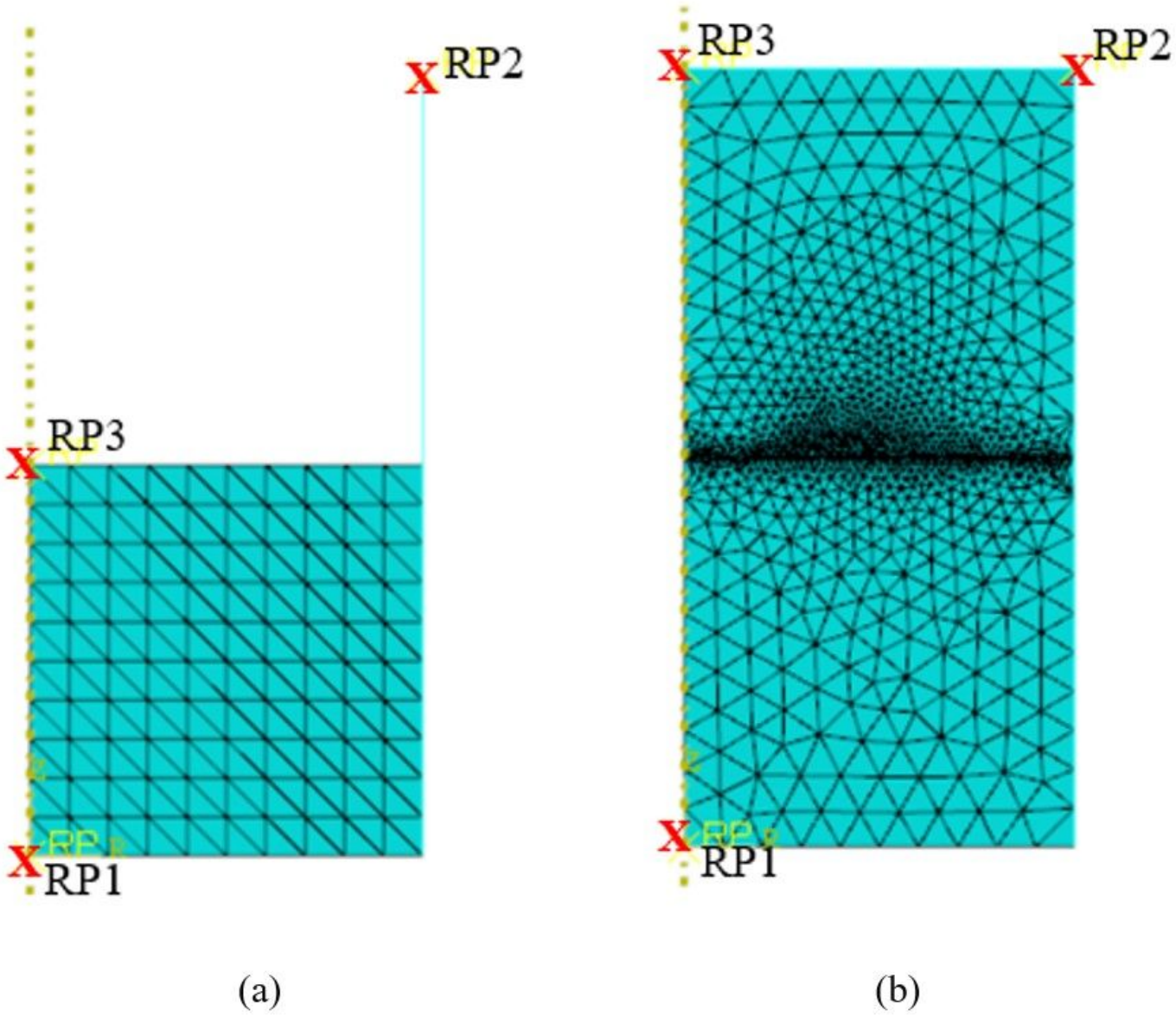

Figure 1

Undeformed axisymmetric model of green (a) single and (b) bilayer iron powder compact.

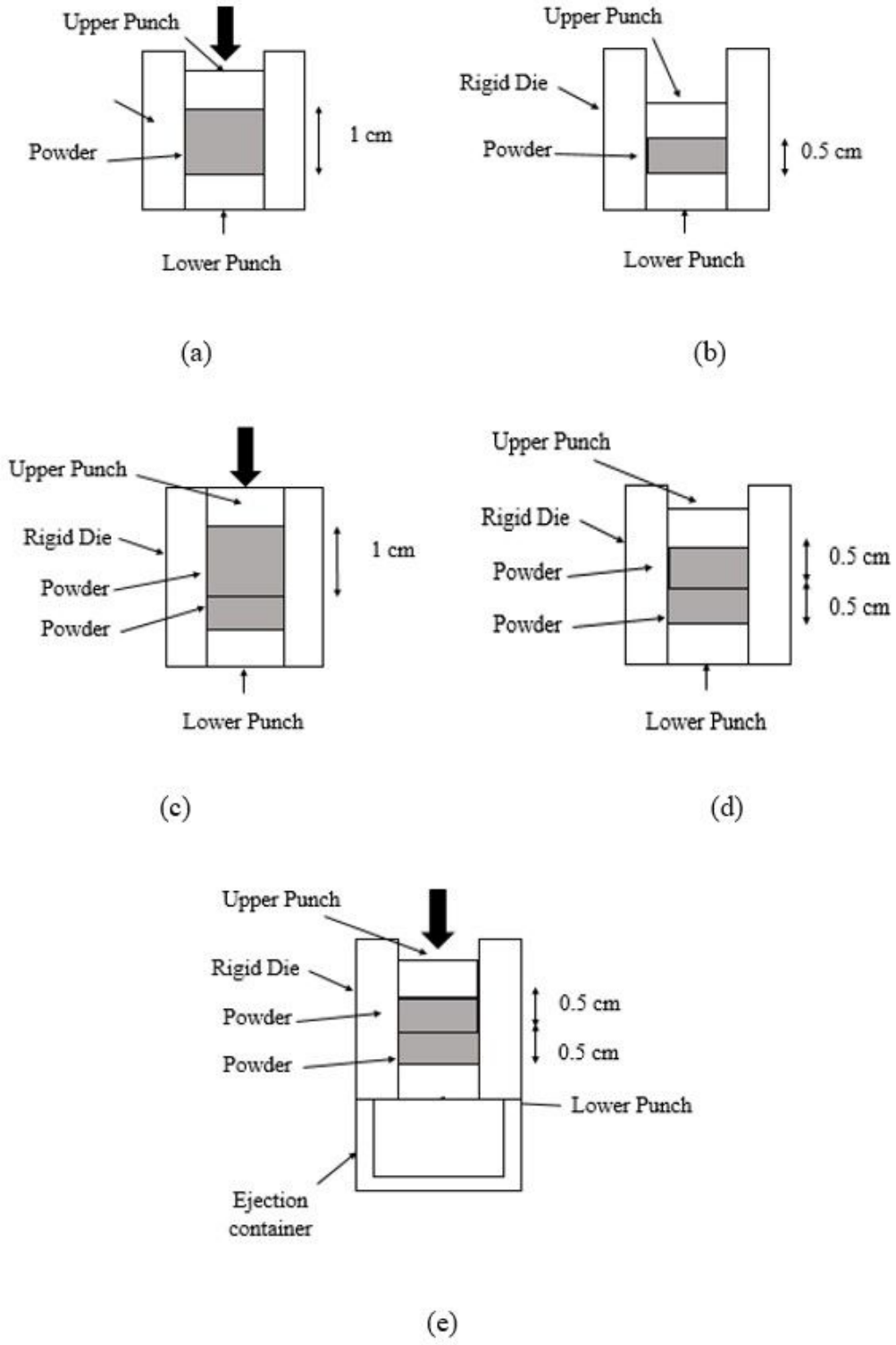

Figure 2

(a)-(d) Compaction and (e) sequence ejection stages to form a green single layer and a bilayer iron powder compact.

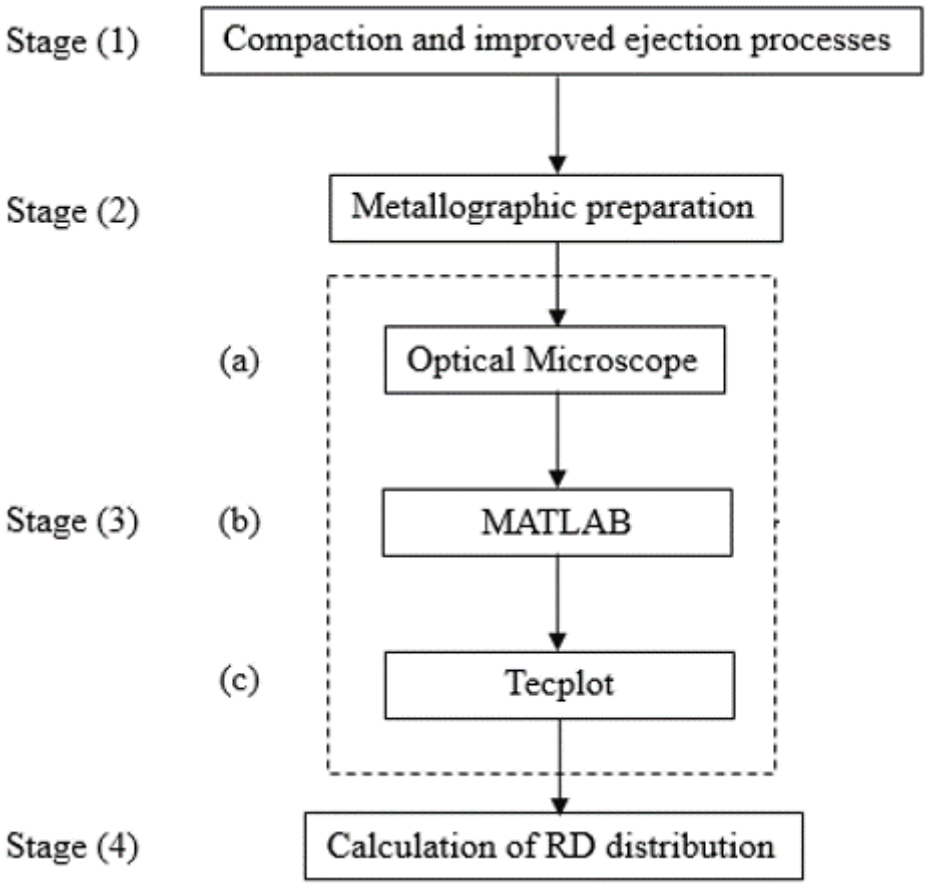

Figure 3

The workflow process to calculate local RD distribution of the cross-sectioned green single and bilayer iron powder compacts.

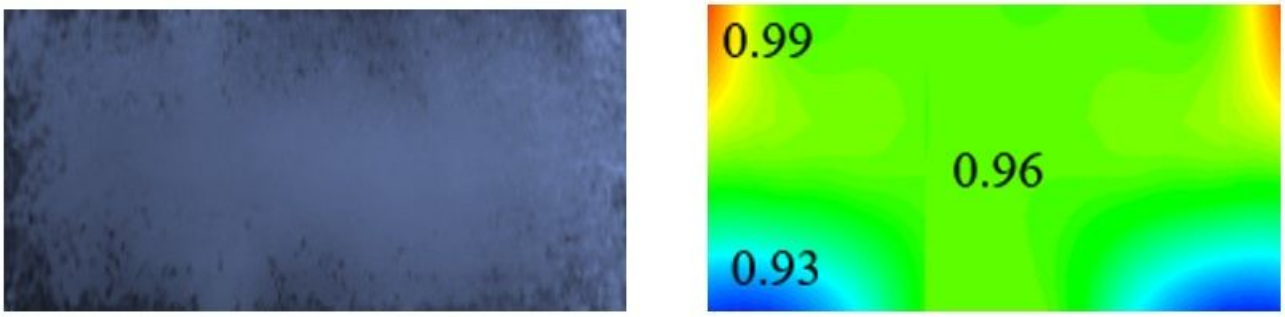

(a) Sample A1

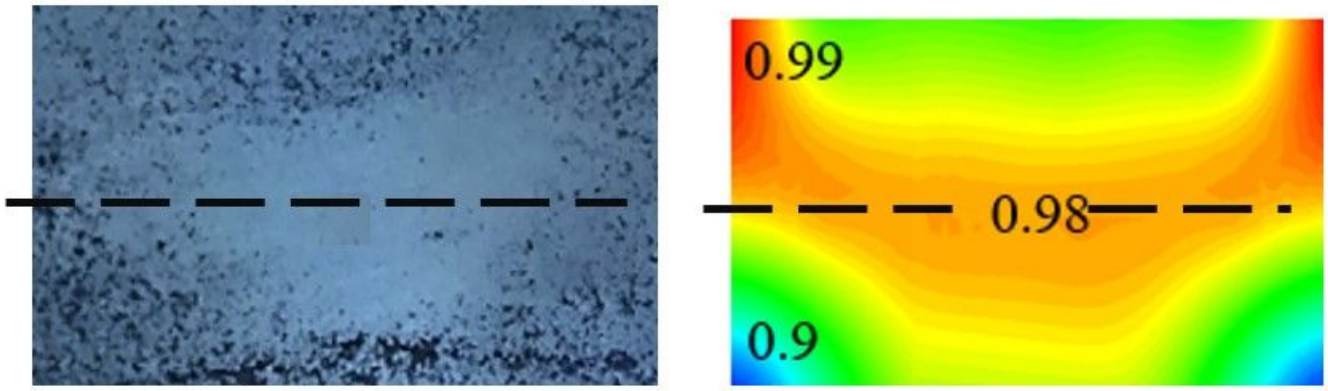

(b) Sample A2

Figure 4

Local RD distributions obtained from experimental work.

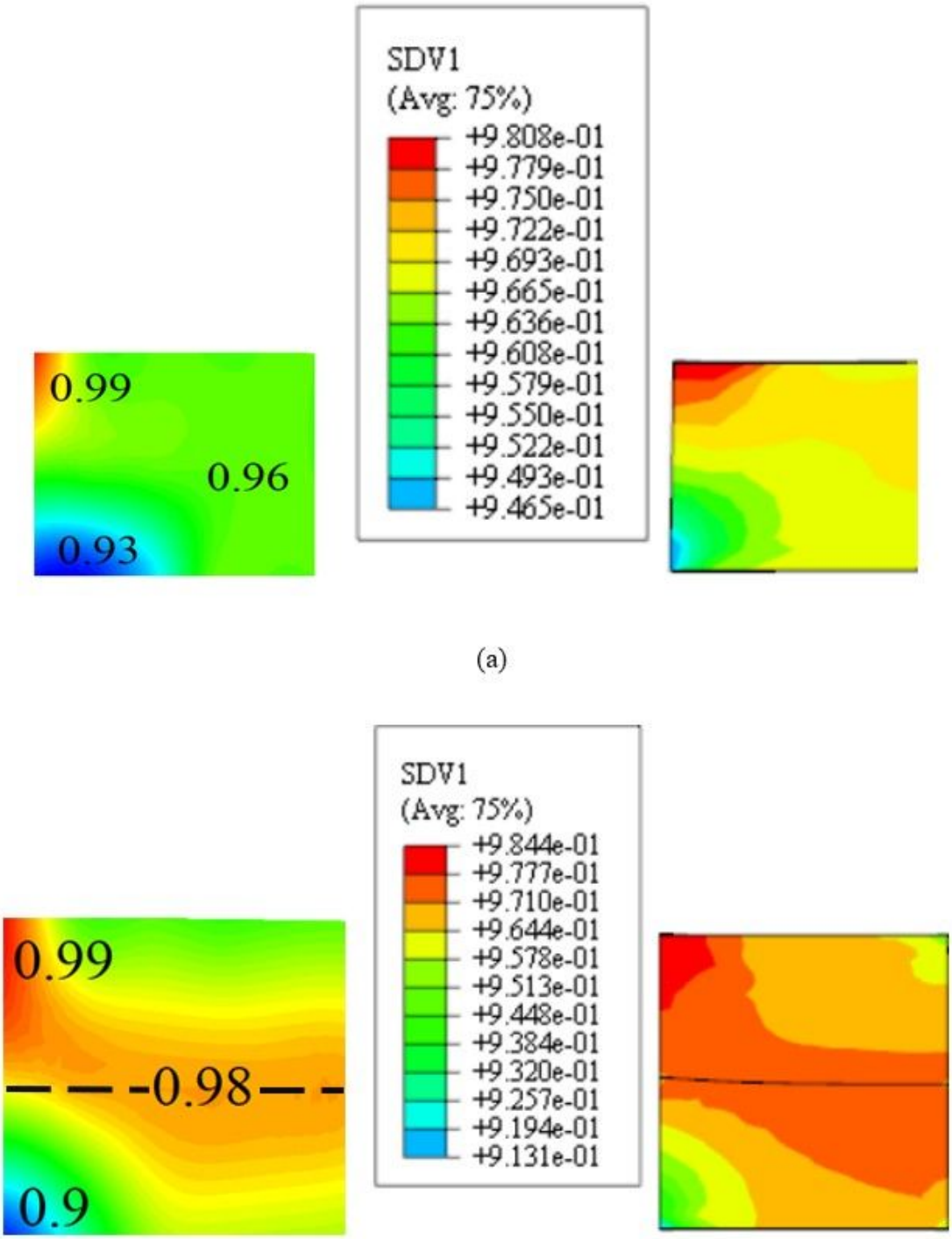

Figure 5

Comparison of RD distributions obtained from the experimental work and FEM for (a) Sample A1 and (b) Sample A2.

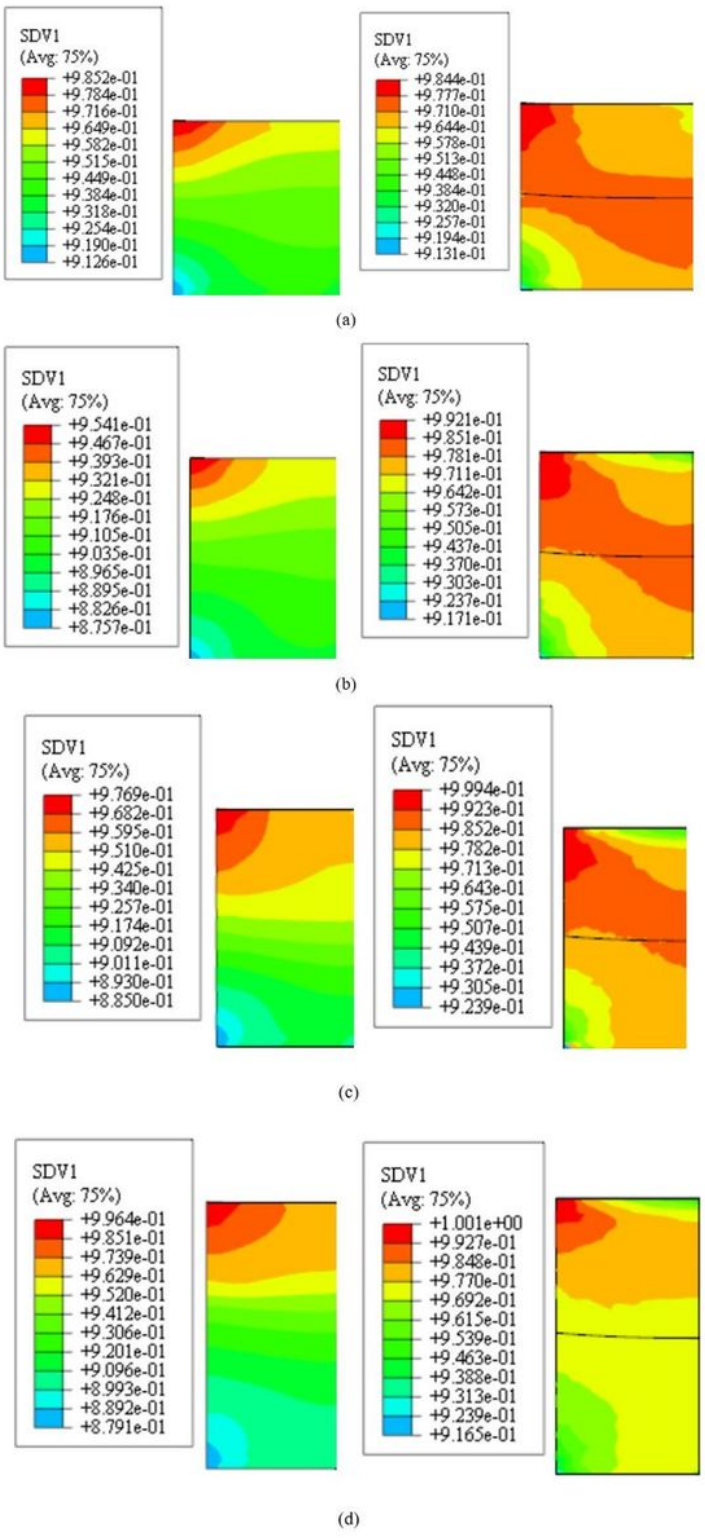

Figure 6

Contour results of local RD distribution as SDV for H/D ratios of: (a) 1.0 (Sample A2), (b) 1.3 (Sample B), (c) 1.6 (Sample C) and (d) 1.9 (Sample D).

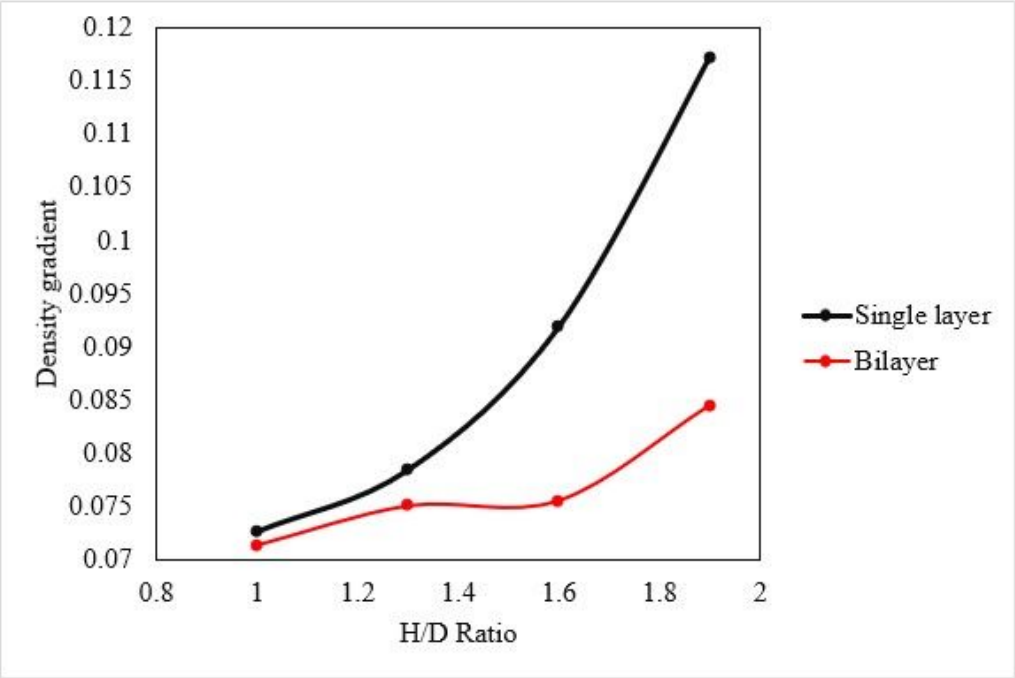

(a)

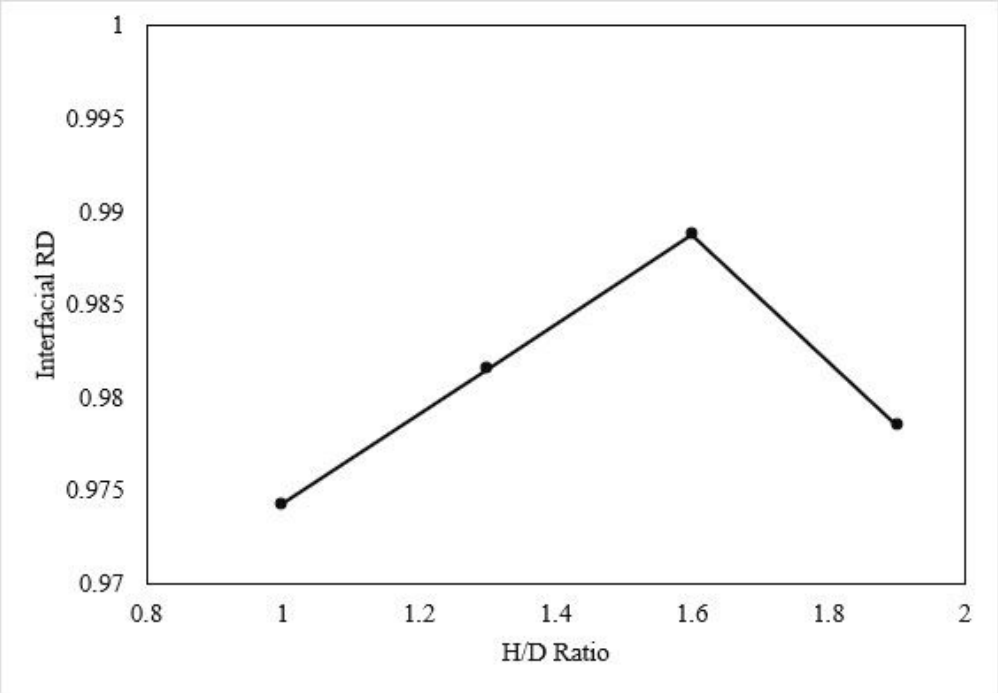

(b)

Figure 7

Graph of: (a) comparison in density gradient for both green single and bilayer and (b) interfacial local RD distribution of green bilayer iron, over H/D ratios of 1.0 (Sample A2), 1.3 (Sample B) and 1.6 (Sample C) and 1.9 (Sample D).